8th GRACM International Congress on Computational Mechanics
Volos, 12 July – 15 July 2015

NON-LINEAR HOMOGENIZATION METHODS FOR THE CONSTITUTIVE MODELING OF MULTIPHASE

I. Papadioti[1,3], K. Danas[2] and N. Aravas[1,4]

[1]Department of Mechanical Engineering
University of Thessaly
Volos, GR-38334, Greece
papadioti@uth.gr, aravas@uth.gr

[2]Laboratoire de Mécanique des Solides, C.N.R.S. UMR7649
École Polytechnique
ParisTech 91128 Palaiseau Cedex, France
kdanas@lms.polytechnique.fr

[3]Institute for Research & Technology --- Thessaly
Centre for Research &Technology Hellas (CERTH)
Volos, GR-38333, Greece

[4] International Institute for Carbon Neutral Energy Research (WPI-I2CNER)
Kyushu University
744 Motooka, Nishi-ku, Fukuoka 819-0395, Japan

Keywords: Multiphase Steels, Plasticity, Finite Element Methods.

Abstract. *Multiphase steels exhibit an excellent combination of strength and ductility, a fact that renders them particularly attractive for automotive applications. A methodology is presented for the development of elastoplastic constitutive equations for multiphase steels in terms of the properties of the constituent phases. The effective properties and overall behavior of steels are determined by using homogenization techniques for non-linear composites. The developed constitutive model considers the hardening behavior of the individual phases and estimates the apportionment of plastic strain and stress in the individual phases involved. A methodology for the numerical integration of the resulting elastoplastic constitutive equations in the context of the finite element method is developed and the constitutive model is implemented in a general-purpose finite element program. A "plane stress" version of the algorithm is developed and a methodology for the calculation of "Forming Limit Diagrams" is presented. The methodology is applied to TRIP steels.*

The predictions of the constitutive models are compared to the results of two- and three-phase three-dimensional isotropic unit cell calculations for different types of loadings, including uniaxial tension and finite shear.

1 INTRODUCTION

A variety of high strength steels like low-alloy dual phase (DP) and TRansformation Induced Plasticity (TRIP) steels have been developed for the automotive industry with respect to the increasing demand for lighter, more deformable, and high energy absorbing materials. These steels exhibit excellent mechanical properties as they combine high strength and good ductility compared to conventional steels of similar strength. This favorable balance of properties is owing to the existence of different phases in their microstructures. In order to exploit the properties of these materials in industrial applications, there is a need for constitutive models that take into account the relation between the microstructure and the mechanical response.

Several authors have developed constitutive models for the mechanical behavior of multiphase steels. Herein, we develop rate-independent constitutive equations for two- and three-phase steels. The total strain is assumed to be the sum of elastic and plastic parts. The plastic part is determined by using homogenization techniques for nonlinear composites that have been developed by Ponte Castañeda (0,0,0).

2 DESCRIPTION OF THE CONSTITUTIVE MODEL

In this section a constitutive model that describes the mechanical behavior of multiphase steels is developed. No restriction is placed on the magnitude of the deformation and appropriate ‘‘finite strain’’ constitutive equations are developed. Each of the phases is assumed to be isotropic, elastic-plastic, and is distributed statistically uniformly and isotropically. The total deformation rate $\mathbf{D}$ is written as the sum of an elastic and a plastic part:

$$\mathbf{D} = \mathbf{D}^e + \mathbf{D}^p \tag{1}$$

2.1 Elastic Constitutive Relations

The elastic properties of all phases are essentially the same and the multiphase steel can be viewed as homogeneous in the elastic region. Standard isotropic linear hypoelasticity is assumed and the constitutive equation for $\mathbf{D}^e$ is written as

$$\mathbf{D}^e = \mathcal{M}^e : \overset{\nabla}{\boldsymbol{\sigma}} \quad \text{or} \quad \overset{\nabla}{\boldsymbol{\sigma}} = \mathcal{L}^e : \mathbf{D}^e \tag{2}$$

where $\overset{\nabla}{\boldsymbol{\sigma}}$ is the Jaumann derivative of the stress tensor $\boldsymbol{\sigma}$, $\mathcal{M}^e$ is the elastic compliance tensor defined as

$$\mathcal{M}^e = \frac{1}{2\mu}\mathbf{K} + \frac{1}{3\kappa}\mathbf{J}, \quad \mathcal{L}^e = \mathcal{M}^{e^{-1}} = 2\mu\mathcal{K} + 3\kappa\mathcal{J}, \quad \mathcal{J} = \frac{1}{3}\boldsymbol{\delta}\boldsymbol{\delta}, \quad \mathcal{K} = I - \mathcal{J} \tag{3}$$

μ and κ denote the elastic shear and bulk moduli, $\boldsymbol{\delta}$ and I the second- and fourth-order identity tensors, with Cartesian components δ_{ij} (the Kronecker delta) and $I_{ijkl} = \left(\delta_{ik}\,\delta_{jl} + \delta_{il}\,\delta_{jk}\right)/2$.

2.2 Constitutive Equations for $\mathbf{D}^p$

The constitutive equations for $\mathbf{D}^p$ are developed as follows. Each phase is assumed to be plastically incompressible and the corresponding constitutive equations are written in terms of a ‘‘viscous stress potentials’’ of the ‘‘power-law’’ type $U^{(r)} = U^{(r)}\left(\sigma_{eq}\right)$:

$$\mathbf{D}^{p(r)} = \frac{\partial U^{(r)}}{\partial \boldsymbol{\sigma}} = \dot{\bar{\varepsilon}}^{p(r)}\,\mathbf{N} = \frac{\mathbf{s}}{2\mu^{(r)}}, \qquad r = 1,..,N \tag{4}$$

$$\text{with} \quad U^{(r)}\left(\boldsymbol{\sigma}\right) = \frac{\sigma_0^{(r)}\,\dot{\varepsilon}_0^{(r)}}{n^{(r)}+1}\left(\frac{\sigma_{eq}}{\sigma_0^{(r)}}\right)^{n^{(r)}+1}, \qquad \mathbf{N} = \frac{3\mathbf{s}}{2\sigma_{eq}}, \qquad \sigma_{eq} = \sqrt{\frac{3}{2}\mathbf{s}:\mathbf{s}} \tag{5}$$

$$\dot{\bar{\varepsilon}}^{p(r)} = \sqrt{\frac{2}{3}\mathbf{D}^{p(r)}:\mathbf{D}^{p(r)}} = \frac{\sigma_{eq}}{3\mu^{(r)}\left(\sigma_{eq}\right)} = \dot{\varepsilon}_0^{(r)}\left(\frac{\sigma_{eq}}{\sigma_0^{(r)}}\right)^{n^{(r)}}, \; \mu^{(r)}\left(\sigma_{eq}\right) = \frac{1}{3}\frac{\sigma_0^{(r)}}{\dot{\varepsilon}_0^{(r)}}\left(\frac{\sigma_0^{(r)}}{\sigma_{eq}}\right)^{n^{(r)}-1} \tag{6}$$

where $\boldsymbol{\sigma}$ is the stress tensor, $\mathbf{s}$ the stress deviator, $\sigma_0^{(r)}$ is a reference stress, $\dot{\varepsilon}_0^{(r)}$ a reference strain rate, $n^{(r)}$ the strain – rate sensitivity exponent, and $\mu^{(r)}\left(\sigma_{eq}\right)$ is the viscous shear modulus.

There are two interesting limiting cases of the model described by equations (4), (5), and (6). The first is the linear case, in which $n^{(r)} = 1$.

$$U_L^{(r)} = \frac{\sigma_0^{(r)}\,\dot{\varepsilon}_0^{(r)}}{2}\left(\frac{\sigma_{eq}}{\sigma_0^{(r)}}\right)^2 = \frac{\sigma_{eq}^2}{6\mu^{(r)}}, \quad \mu^{(r)} = \frac{\sigma_0^{(r)}}{3\dot{\varepsilon}_0^{(r)}}, \quad \dot{\bar{\varepsilon}}^{p(r)} = \frac{\sigma_{eq}}{3\mu^{(r)}} = \dot{\varepsilon}_0^{(r)}\frac{\sigma_{eq}}{\sigma_0^{(r)}} \tag{7}$$

The second limiting case is perfect plasticity in which $n^{(r)} \to \infty$. Taking into account that

$$\lim_{n\to\infty} \frac{A^{n+1}}{n+1} = \begin{cases} 0 & \text{if} \quad A \le 1, \\ \infty & \text{if} \quad A > 1, \end{cases} \tag{8}$$

we conclude that

$$U^{(r)} = \lim_{n^{(r)}\to\infty} \left[\frac{1}{n^{(r)}+1} \sigma_0^{(r)} \dot{\varepsilon}_0^{(r)} \left(\frac{\sigma_{eq}}{\sigma_0^{(r)}} \right)^{n^{(r)}+1} \right] = \begin{cases} 0 & \text{if} \quad \dfrac{\sigma_{eq}}{\sigma_0^{(r)}} \le 1, \\ \infty & \text{if} \quad \dfrac{\sigma_{eq}}{\sigma_0^{(r)}} > 1. \end{cases} \tag{9}$$

Our goal is to determine the corresponding viscoplastic constitutive equation for the ‘‘composite’’ multiphase steel, i.e., an equation of the form $\mathbf{D}^p = \mathbf{D}^p(\boldsymbol{\sigma})$, and then consider the rate-independent limit. This is achieved in three steps.

First step

The dissipation function of the composite is defined by (0,0)

$$\tilde{U}(\bar{\boldsymbol{\sigma}}) = \sup_{\mu^{(r)}\ge 0} \left\{ \tilde{U}_L\left(\bar{\sigma}_{eq}, \tilde{\mu}\left(\mu^{(r)}\right)\right) - \sup_{\sigma_{eq}^{(r)}\ge 0} \sum_{r=1}^{4} c^{(r)} \left[U_L^{(r)}\left(\sigma_{eq}^{(r)}, \mu^{(r)}\right) - U^{(r)}\left(\sigma_{eq}^{(r)}\right) \right] \right\} \tag{10}$$

where $\tilde{U}_L = \bar{\sigma}_{eq}^2 / \left[6\,\tilde{\mu}\left(\mu^{(r)}\right) \right]$ is the dissipation potential of a “linear comparison composite”. The corresponding constitutive equation for the composite is

$$\bar{\mathbf{D}} = \frac{\partial \tilde{U}}{\partial \bar{\boldsymbol{\sigma}}} \tag{11}$$

where $\bar{\boldsymbol{\sigma}}$ and $\bar{\mathbf{D}}$ are the macroscopic stress and deformation rate tensors respectively. The effective modulus $\tilde{\mu}$ for particulate composites is estimated in terms of a reference modulus μ_0 as

$$\tilde{\mu}\left(\mu^{(r)}\right) = \frac{\displaystyle\sum_{s=1}^{N} c^{(s)}\,\mu^{(s)} \left(3\mu_0 + 2\mu^{(s)}\right)^{-1}}{\displaystyle\sum_{r=1}^{N} c^{(r)} \left(3\mu_0 + 2\mu^{(r)}\right)^{-1}} \tag{12}$$

where μ_0 is defined using the Reuss model $\left(\dfrac{1}{\mu_0} = \displaystyle\sum_{r=1}^{N} \frac{c^{(r)}}{\mu^{(r)}} \right)$.

Second step

All creep exponents are set equal, i.e. $n^{(1)} = n^{(2)} = \cdots = n^{(N)} \equiv n$. Then the optimization problem (10) reduces to

$$\tilde{U} = \frac{\bar{\sigma}_{eq}^{n+1}}{n+1} \sqrt{ \sup_{y^{(r)}\ge 0} \left\{ \frac{\left[F\left(y^{(r)}\right) \right]^{n+1}}{\left[H^n\left(y^{(r)}\right) \right]^{n-1}} \right\}}, \qquad y^{(r)} = \frac{\mu^{(1)}}{\mu^{(r)}} \tag{13}$$

where $F\left(y^{(r)}\right)=\dfrac{\mu^{(1)}}{\tilde{\mu}}=\dfrac{\displaystyle\sum_{r=1}^{N}c^{(r)}\,y^{(r)}\left(3\dfrac{y^{(r)}}{y_0}+2\right)^{-1}}{\displaystyle\sum_{s=1}^{N}c^{(s)}\left(3\dfrac{y^{(s)}}{y_0}+2\right)^{-1}}$ and $H\left(y^{(r)}\right)=\displaystyle\sum_{r=1}^{N}c^{(r)}\left[\frac{\left(\sigma_0^{(r)}\right)^n}{\dot{\varepsilon}_0^{(r)}}\right]^{\frac{2}{n-1}}\left(y^{(r)}\right)^{\frac{n+1}{n-1}}$

Third step

We consider the limit $n\to\infty$ and (13) takes the form

$$\tilde{U}=\begin{cases}0 \quad \text{when} \quad \bar{\sigma}_{eq}^2\ \displaystyle\sup_{\substack{y^{(r)}\geq 0\\ y^{(1)}=1}}\left[\frac{F\left(y^{(r)}\right)}{H^{\infty}\left(y^{(r)}\right)}\right]\leq 1,\\ \infty \quad \text{when} \quad \bar{\sigma}_{eq}^2\ \displaystyle\sup_{\substack{y^{(r)}\geq 0\\ y^{(1)}=1}}\left[\frac{F\left(y^{(r)}\right)}{H^{\infty}\left(y^{(r)}\right)}\right]>1.\end{cases} \tag{14}$$

Comparing the above equation with (9) we conclude that the composite material obeys a von-Mises-like yield criterion with a flow stress $\bar{\sigma}_0$ defined by

$$\bar{\sigma}_0=\sqrt{\inf_{\substack{y^{(r)}\geq 0\\ y^{(1)}=1}}\left[\sum_{t=1}^{N}c^{(t)}\left(\sigma_0^{(t)}\right)^2 y^{(t)}\left(\sum_{s=1}^{N}\frac{c^{(s)}}{3\dfrac{y^{(s)}}{y_0}+2}\right)\left(\sum_{r=1}^{N}\frac{c^{(r)}\,y^{(r)}}{3\dfrac{y^{(r)}}{y_0}+2}\right)^{-1}\right]} \tag{15}$$

where $c^{(r)}$ are the volume fraction of the phases. This is the end of the third step.

The average deformation rate $\bar{\mathbf{D}}^{(r)}$ over each phase is determined from the macroscopic deformation rate $\bar{\mathbf{D}}$ in terms of a "strain concentration tensor" $\mathbf{A}^{(r)}$ ([3], [4], [5]):

$$\bar{\mathbf{D}}^{(r)}=\mathbf{A}^{(r)}:\bar{\mathbf{D}} \tag{16}$$

where in the present case

$$\bar{\mathbf{D}}^{(i)}=\mathbf{A}^{(i)}:\bar{\mathbf{D}}=\frac{y^{(i)}}{3y^{(i)}+2y_0}\left(\sum_{s=1}^{N}\frac{c^{(s)}\,y^{(s)}}{3y^{(s)}+2y_0}\right)^{-1}\bar{\mathbf{D}}\equiv\alpha^{(i)}\,\bar{\mathbf{D}} \tag{17}$$

The above formulation is rigorous when all phases are perfectly plastic. In our applications, the analysis is carried out incrementally and the yield stresses of the phases are updated at each increment.

Note that the calculation of the effective yield stress $\bar{\sigma}_0$ in (15) involves a constrained minimization problem. This is solved by using the methodology developed by Kaufman *et al.* 0 and the CONMAX software (http://www.netlib.org/opt/conmax.f).

3 APPLICATIONS

A methodology for the numerical integration of the constitutive model is developed and implemented in the ABAQUS general purpose finite element program. ABAQUS provides a general interface so that a particular constitutive model can be introduced as a ''user subroutine'' (UMAT). The finite element formulation is based on the weak form of the momentum balance, the solution is carried out incrementally, and the discretized nonlinear equations are solved using Newton's method.

3.1 The Example of a Two-Phase Composite

In order to check the proposed model, we consider a simple two-phase system with $c^{(1)} = 0.6$, $c^{(2)} = 0.4$, and $\sigma_0^{(2)} / \sigma_0^{(1)} = 5$, phase-1 being the matrix material. The predictions of the model are compared to the results of three-dimensional isotropic unit-cell calculations for uniaxial tension and finite shear in Figure 1. The unit cell is cubic with a random distribution of a large number of spherical particles. The hardening curves $\left(\sigma_y^{(i)}\right)$ of the two phases are (in MPa):

$$\sigma_y^{(1)} = 240 + 730\left(\bar{\varepsilon}^{p(1)}\right)^{0.47} \quad \text{and} \quad \sigma_y^{(2)} = 1200 + 1500\left(\bar{\varepsilon}^{p(2)}\right)^{0.23} \tag{18}$$

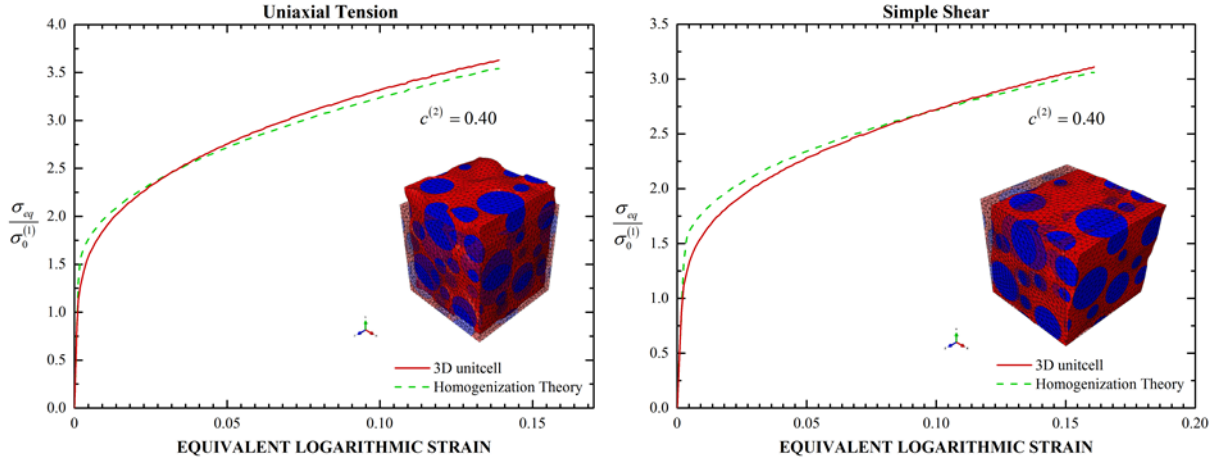

Figure 1. Stress-strain curves of a two-phase composite for (a) uniaxial tension and (b) simple shear.

3.2 The Example of a Three-Phase Composite

In this section, we consider a three-phase system with $c^{(1)} = 0.6$, $c^{(2)} = 0.25$ and $c^{(3)} = 0.15$, phase-1 being the matrix material. The results are shown in Figure 2. The hardening curves $\left(\sigma_y^{(i)}\right)$ of the two phases are (in MPa):

$$\sigma_y^{(1)} = 240 + 730\left(\bar{\varepsilon}^{p(1)}\right)^{0.47}, \quad \sigma_y^{(2)} = 810 + 1400\left(\bar{\varepsilon}^{p(2)}\right)^{0.43} \quad \text{and} \quad \sigma_y^{(3)} = 1200 + 1500\left(\bar{\varepsilon}^{p(3)}\right)^{0.23} \tag{19}$$

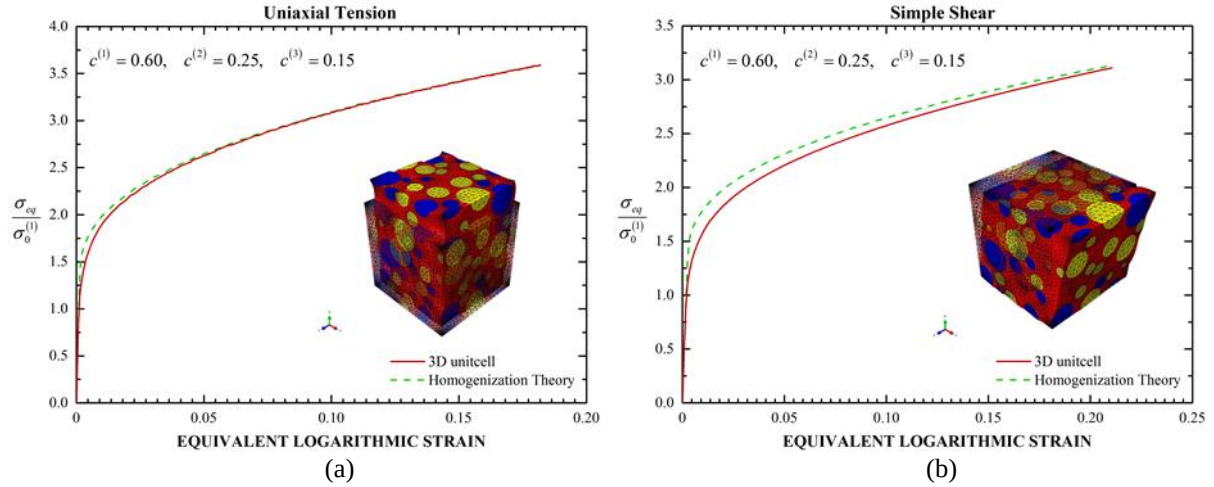

Figure 2. Stress-strain curves of a three-phase composite for (a) uniaxial tension and (b) simple shear.

3.3 Necking of a bar

In this section, we study the development of a neck in a TRIP specimen in a uniaxial tension test. The TRIP steel consists of a ferritic matrix (1) with dispersed bainite (2) and austenite (3), which transforms gradually into martensite (4) as the material deforms plastically. From a mathematical point of view, necking is a bifurcation of the uniform solution to the problem. Bifurcation analyses are usually replaced by studies of the sensitivity of the solution to small imperfections of some sort. Such an imperfection approach is used here in order to study the development of a neck in a tension specimen.

We consider a cylindrical specimen with aspect ratio $L_0 / R_0 = 3$, where $2\,L_0$ is its initial length and R_0 its initial radius. Because of symmetry, only one half of the cylindrical specimen is analysed. The deformation is driven by the uniform prescribed end displacement in the axial direction on the shear free end while the lateral surface of the specimen is kept traction free. In order to promote necking, a geometric imperfection of the following form is introduced:

$$R(z) = R_0 - \xi\, R_0 \cos\frac{\pi\, z}{2\, L_0} \tag{20}$$

where $R(z)$ is the perturbed radius of the specimen, the value $\xi = 0.005$ is used and the plane $z = 0$ coincides with the middle cross section of the specimen. The details of the formulation are given in Papatriantafillou *et al*. 0. The initial volume fractions are $c^{(1)} = 0.50$, $c^{(2)} = 0.38$, $c^{(3)} = 0.103$, and $c^{(4)} = 0.017$.

The hardening curves $\left(\sigma_y^{(i)}\right)$ of the four phases are (in MPa):

$$\begin{aligned} \sigma_y^{(1)} &= 240 + 730\left(\bar{\varepsilon}^{\,p(1)}\right)^{0.47}, & \sigma_y^{(2)} &= 810 + 1400\left(\bar{\varepsilon}^{\,p(2)}\right)^{0.43} \\ \sigma_y^{(3)} &= 450 + 900\left(\bar{\varepsilon}^{\,p(3)}\right)^{0.46}, & \sigma_y^{(4)} &= 1200 + 1500\left(\bar{\varepsilon}^{\,p(4)}\right)^{0.23} \end{aligned} \tag{21}$$

For comparison purposes, a separate set of calculations is carried out at room temperature for a non-transforming TRIP steel with the same initial values of the volume fractions of the four phases.

Figure 3 shows the stress-strain curves for both a transforming and a non-transforming material at room temperature. The arrows on the curves indicate the point of maximum load, which coincides with end of uniform elongation of the specimen. For the transforming (TRIP) steel the end of uniform elongation is observed at a nominal strain of 31% and 772 MPa stress, whereas for the non-transforming steel at 28% and 729 MPa. Figure 3 makes it clear that the TRIP effect not only hardens the material but also increases substantially the range of uniform elongation.

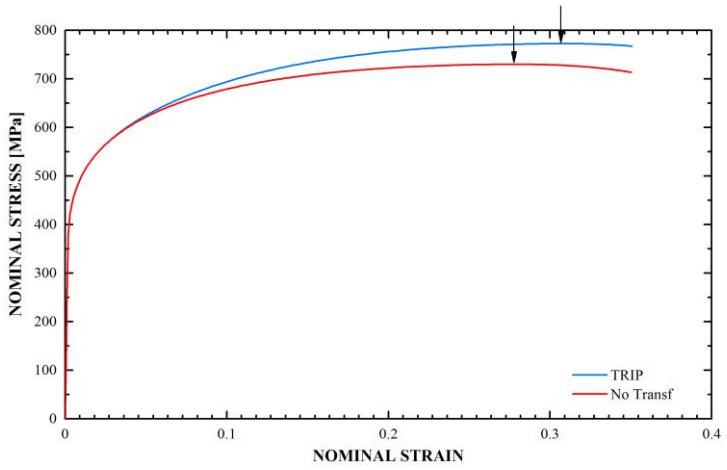

Figure 3. Stress-strain curves for a TRIP steel and a non-transforming steel at room temperature. Arrows indicate maximum-load position.

Figure 4 shows the deformed configurations for the transforming and non-transforming materials at a nominal strain level of 50%. The formation of martensite stabilizes the neck and leads to its propagation down the length of the specimen. At a nominal strain of 50%, the non-transforming material exhibits a 53.3% reduction of its minimum cross section; the corresponding reduction for the TRIP steel is 46.3%.

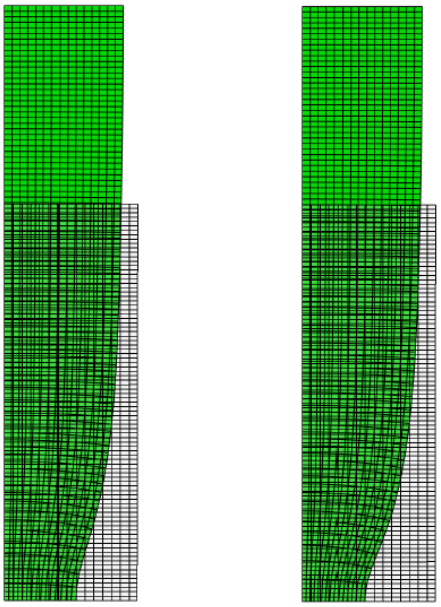

(a) (b)

Figure 4. Deformed configurations for a nominal strain of 50% at room temperature: (a) transforming , (b) non-transforming steel.

3.4 Forming Limit Diagrams

We consider a sheet made of TRIP steel that is deformed uniformly on its plane in such a way that the in-plane principal strain increments increase in proportion. We study the possibility of the formation of a neck in the form of a narrow straight band and construct the corresponding ‘‘forming limit diagram’’. The details of the formulation are given in Papatriantafillou *et al.* 0. The initial volume fractions are $c^{(1)} = 0.50$, $c^{(2)} = 0.38$, $c^{(3)} = 0.103$, and $c^{(4)} = 0.017$.

We follow the approach of Marciniak and Kuzynski 0, known as the ‘‘M–K’’ model, in which the sheet is assumed to contain a small initial inhomogeneity and necking results from a gradual localization of the strains at the inhomogeneity. The inhomogeneity is in the form of straight narrow band (neck) of reduced thickness $H^b < H$. Both inside and outside the band a state of uniform plane stress is assumed, and the analysis consists in determining the uniform state of deformation inside the band that is consistent kinematically and statically with the prescribed uniform state outside the band. Given the initial sheet thickness inside and outside the band and the imposed uniform deformation history outside the band, the equations of equilibrium are solved incrementally to obtain the deformation history inside the band. Localization is said to occur when the ratio of some scalar measure of the amount of incremental straining inside the band to the corresponding value outside the band becomes unbounded.

Figure 5 shows forming limit curves obtained for imposed proportional straining for two different values of the initial thickness imperfection, namely $H^b / H = 0.999$ and $H^b / H = 0.99$ and for the case without imperfection i.e. $H^b = H = 1$. In particular, the curves in Figure 5 show the values of the strains $\varepsilon_1 = \varepsilon_1^{cr}$ and $\varepsilon_1^{cr} = \rho\,\varepsilon_2^{cr}$ at which necking takes place for different values of ρ. The three solid curves correspond to the TRIP steel, whereas the dashed curves are for the non-transforming steel. In particular, for no imperfection and $\rho = 0$ (plane strain), the critical strain ε_1^{cr} increases from 0.2685 for the non-transforming steel to 0.2892 for the TRIP steel; the corresponding values of ε_1^{cr} for $H^b / H = 0.999$ and $\rho = 0$ are 0.2438 for the non-transforming steel and

0.2653 for the TRIP steel and for $H^b / H = 0.99$ and $\rho = 0$ are 0.1952 for the non-transforming steel and 0.2179 for the TRIP steel. A comparison of the model predictions with available experimental data is also presented in Figure 5. The experimental points on the forming limit diagram were determined for the same TRIP steel used for the calibration of the model. The agreement between the model predictions and the experimental data is reasonable.

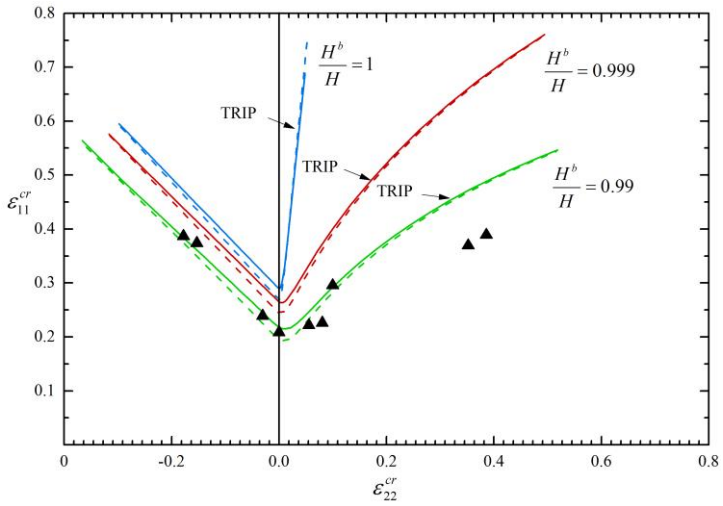

Figure 5. Forming limit curves for two different values of initial thickness inhomogeneities $H^b / H = 0.999$ and $H^b / H = 0.99$. The solid lines correspond to the TRIP steel, whereas the dashed lines are for a non-transforming steel. The dark triangles are experimental data.

ACKNOWLEDGEMENTS

This work was carried out while the authors were supported by the Greek General Secretariat for Research and Technology (GSRT) through the ΚΡΗΠΙΣ Project.

REFERENCES

[1] Ponte Castañeda P. (1991), "The effective mechanical properties of nonlinear isotropic solids", *Journal of the Mechanics and Physics of Solids*, Vol. 39, pp. 45−71.

[2] Ponte Castañeda P. (1992), "New variational principles in plasticity and their application to composite materials", *Journal of the Mechanics and Physics of Solids*, Vol. 40, pp. 1757−l788.

[3] Ponte Castañeda P. (1997), "Nonlinear composite materials: effective constitutive behavior and microstructure evolution". *In: Continuum Micromechanics, CISM Courses and Lectures*, ed. P. Suquet, Vol. 377, pp. 13l−l95. Springer-Verlag.

[4] Kailasam M. and Ponte Castañeda P. (1998), "A general constitutive theory for linear and nonlinear particulate media with microstrucure evolution", *Journal of the Mechanics and Physics of Solids*, Vol. 46, pp. 427−465.

[5] Ponte Castañeda P. and Suquet P. (1998), "Nonlinear composites", *Advances in Applied Mechanis*, Vol. 34, pp. 171−303.

[6] Kaufman E.H., Leeming D.J., and Taylor G.D. (1995), "An ODE-based approach to nonlinearly constrained problems". *Numerical Algorithms*, Vol. 9, pp. 25−37.

[7] Papatriantafillou I., Agoras M., Aravas N., and Haidemenopoulos G. (2006), "Constitutive modeling and finite element methods for TRIP steels", *Comput. Methods Appl. Mech. Engrg*., Vol. 195, pp. 5094−5114.

[8] Marciniak Z. and Kuczynski K. (1967), "Limit strains in the process of stretch forming sheet metal". *Int. J. Mech. Sci.*, Vol. 9, pp. 609–620.